

PHOTOABSORPTION ON A NUCLEON IN THE D_{13} RESONANCE ENERGY REGION

Kazuyuki OCHI ^{*}, Michihiro HIRATA

Department of Physics, Hiroshima University, Higashi-Hiroshima 739, Japan

and

Takashi TAKAKI

Onomichi Junior College, Onomichi 722, Japan

Abstract

We present a simple model for the $\gamma N \rightarrow \pi\pi N$ reaction which reproduces the cross sections of the $\pi^+\pi^-p$, $\pi^+\pi^-n$, $\pi^+\pi^0n$ and $\pi^-\pi^0p$ channels over the range of the energies 0.41–0.85 GeV. We use the dynamical model for the resonances, $\Delta(1232)$, $N^*(1520)$ and ρ -meson. The total photoabsorption off a nucleon is also discussed.

PACS number(s): 25.20.Dc, 25.20.Lj

Typeset using REVTeX

^{*}e-mail: kazu@theo.phys.sci.hiroshima-u.ac.jp

I. INTRODUCTION

The total nuclear-photoabsorption cross sections through the third resonance (0.2 – 1.2 GeV photon laboratory energy) have been measured for a wide set of nuclei to study the behavior of baryon resonances [1–5] in nuclear matter. These measurements show an interesting result. In the first resonance region, the P_{33} resonance ($l = 1, J = 3/2, I = 3/2$) is slightly distorted. In the second and third resonance region, on the other hand, the total cross section is largely suppressed and the resonances such as $D_{13}(l = 2, J = 3/2, I = 1/2)$ and $F_{15}(l = 3, J = 5/2, I = 1/2)$ disappear in the excitation function. Apparently, these resonances in the fundamental process, i.e., pion photoproduction off a nucleon, are strongly modified by nuclear medium effects. There have been several theoretical works [6–8] to explain the disappearance of the resonances. In some phenomenological analyses [6,7], very large collision broadening have been assumed to fit the data. In the other work [8], however, it has been claimed that such significantly increasing resonance widths were hardly justified. The puzzle regarding the mechanism of resonance disappearance still remains unresolved.

In the D_{13} and F_{15} resonance regions, the double pion photoproduction ($\gamma N \rightarrow \pi\pi N$) is important on pion photoproduction in addition to the single pion photoproduction ($\gamma N \rightarrow \pi N$). In those processes, the $N^*(1520)(J^P = 3/2^-, I = 1/2)$ and the $N^*(1680)(J^P = 5/2^+, I = 1/2)$ resonances play a significant role as an intermediate state. In order to investigate the unknown mechanism that has caused resonances damping, one needs precise information about those fundamental pion photoproduction processes.

The $\gamma N \rightarrow \pi N$ reaction has been studied experimentally in the past [9]. Moorhouse *et al.* [10] and Arai *et al.* [11] analyzed the $\gamma N \rightarrow \pi N$ reaction data from the first through the third resonance region. They made a partial-wave analysis of the processes $\gamma p \rightarrow \pi^+ n$, $\gamma p \rightarrow \pi^0 p$, and $\gamma n \rightarrow \pi^- p$. The imaginary parts of the amplitudes were parameterized with K -matrices written as a sum of factorizable poles. The real parts of the amplitudes are calculated from the imaginary parts through the fixed- t dispersion relations. Furthermore, Arndt *et al.* [12] made an energy-dependent partial-wave analysis on the data for the processes $\gamma p \rightarrow \pi^+ n$,

$\gamma p \rightarrow \pi^0 p$, $\gamma n \rightarrow \pi^- p$, $\gamma n \rightarrow \pi^0 n$ and the inverse reaction $\pi^- p \rightarrow n\gamma$. From their analyses, D_{13} and F_{15} resonances have been found to be important in the $\gamma N \rightarrow \pi N$ reaction in addition to the P_{33} resonance.

The $\gamma p \rightarrow \pi^+ \pi^- p$ reaction cross section has been measured as a function of the photon energy (0.3 – 5.8 GeV) by ABBHHM collaboration in 1968 [13]. Recently, new improvement in experimental techniques make them possible to study the $\gamma p \rightarrow \pi^+ \pi^- p$ more accurately and to observe other isospin channels, i.e., $\gamma p \rightarrow \pi^0 \pi^+ n$ and $\gamma p \rightarrow \pi^0 \pi^0 p$. These new data have been obtained at Mainz for photon energy ranging 0.45 – 0.8 GeV [14]. Theoretically, the $\gamma N \rightarrow \pi\pi N$ reactions were studied by Tejedor *et al.* [15] and Murphy *et al.* [16]. Their studies show that their models can reproduce the $\gamma p \rightarrow \pi^+ \pi^- p$ reaction cross sections fairly well, but fail to explain the $\gamma p \rightarrow \pi^+ \pi^0 n$ cross section. Tejedor *et al.*, furthermore, calculated the cross sections for the neutron target, but the results are not in good agreement with the data [17,18]. In order to investigate the total nuclear photoabsorption cross section, their models should be improved.

In this paper we propose a modified model for the $\gamma N \rightarrow \pi\pi N$ reaction, taking into account both $\gamma N \rightarrow \pi N$ and $\gamma N \rightarrow \pi\pi N$ reactions consistently and treating the ρ -meson propagation carefully. The self-energy of the ρ -meson is calculated assuming the $\rho\pi\pi$ form factor. We focus on the photon energy range measured at Mainz [14]. So, we include only the $\Delta(1232)$ and $N^*(1520)$ as intermediate baryon resonance states in our model. The $N^*(1520)$ will be treated carefully since it contributes importantly to the $\gamma N \rightarrow \pi N$ and $\gamma N \rightarrow \pi\pi N$ reactions. The dominant Δ Kroll-Ruderman term is constructed from the finite-ranged form factor of the $\pi N \Delta$ by requiring the gauge invariance.

This paper is organized as follows. In Sec.II we discuss how to describe the D_{13} amplitude and the $N^*(1520)$ propagator and furthermore how to determine strong coupling constants such as $\pi NN^*(1520)$, $\pi\Delta N^*(1520)$ and $\rho NN^*(1520)$ in detail. In Sec.III we discuss how to obtain the $\gamma NN^*(1520)$ coupling constant. In Sec.IV we present our model of the $\gamma N \rightarrow \pi\pi N$ reaction, which is based on the formalism given in Secs.II and III. In Sec.V, we show our predictions of the $\gamma N \rightarrow \pi\pi N$ cross sections and the total photoabsorption cross sections

and then we discuss the numerical results. Finally we give concluding remarks in Sec.VI.

II. $N^*(1520)$ RESONANCE

The $N^*(1520)$ resonance can decay into both the πN and $\pi\pi N$ channels. The branching fractions to πN and $\pi\pi N$ are 50~60% and 40~50% [19], respectively. The $\pi\pi N$ decay occurs through three different modes, i.e., $\pi\Delta$, ρN and $N(\pi\pi)_{\text{s-wave}}^{I=0}$. The $\pi\Delta$ channel is in either s-wave or d-wave state. The branching fractions of the s-wave and d-wave decays are 5~12% and 10~14%, respectively. The branching fraction to ρN is 15~25% and $N(\pi\pi)_{\text{s-wave}}^{I=0}$ is almost negligible. For simplicity, hereafter we denote $N^*(1520)$ as N^* .

Bhalerao *et al.* [20] and Arima *et al.* [21] constructed the isobar model so as to describe the πN scattering in the D_{13} channel. In this model, the N^* resonance is treated as the isobar state. The self-energy of N^* should include the contributions of both πN and $\pi\pi N$ channels as known from the Particle Data [19]. In their models, the $\pi\pi N$ channel was effectively regarded as the $\pi\Delta$ channel. We extend their models to apply to the pion photoproduction. We explicitly include three important decay modes, i.e., s- and d-wave $\pi\Delta$ and ρN , in the $\pi\pi N$ decay channel, since each of such modes plays a significant role in the double pion photoproduction process. This will be discussed later in detail.

In the isobar model, the πN t -matrix in the D_{13} channel is written as

$$t = \frac{F_{\pi NN^*} F_{\pi NN^*}^\dagger}{\sqrt{s} - M_{N^*}^0 - \Sigma_{\text{total}}}, \quad (2.1)$$

where \sqrt{s} and $M_{N^*}^0$ denote the total energy in the center-of-mass system and the bare mass of N^* , respectively. The total self-energy of N^* , i.e., Σ_{total} , is expressed as

$$\Sigma_{\text{total}} = \Sigma_{\pi N} + \Sigma_{\pi\Delta}^s + \Sigma_{\pi\Delta}^d + \Sigma_{\rho N}, \quad (2.2)$$

where $\Sigma_{\pi N}$, $\Sigma_{\pi\Delta}^s$, $\Sigma_{\pi\Delta}^d$ and $\Sigma_{\rho N}$ are due to the coupling to the πN , s-wave $\pi\Delta$, d-wave $\pi\Delta$ and ρN channels, respectively.

The vertex function for the $\pi N \rightarrow N^*$ is written as

$$F_{\pi NN^*}^\dagger = -i(2\pi)^{3/2} \sqrt{\frac{2\omega_\pi(p)E_N(p)}{M}} \frac{f_{\pi NN^*}}{\sqrt{2(m+M)}} \left(\frac{p}{p_{\pi NN^*}}\right)^2 e^{-(p/p_{\pi NN^*})^2} \left(S^{(2)\dagger} \cdot Y_2(\hat{\mathbf{p}})\right), \quad (2.3)$$

where \mathbf{p} and $\hat{\mathbf{p}}$ are the pion momentum and its unit-vector in the πN center-of-mass system, respectively and $\omega_\pi(p) = \sqrt{m^2 + |\mathbf{p}|^2}$, $E_N(p) = \sqrt{M^2 + |\mathbf{p}|^2}$ and $p = |\mathbf{p}|$. $f_{\pi NN^*}$ is the πNN^* coupling constant and $p_{\pi NN^*}$ is the πNN^* range parameter, and M and m denote nucleon and pion masses, respectively. $S^{(2)\dagger}$ in Eq.(2.3) is defined by

$$S^{(2)\dagger} = \sqrt{\frac{2}{5}} \left[\mathbf{S}^\dagger \times \boldsymbol{\sigma} \right]^{(2)}, \quad (2.4)$$

where \mathbf{S}^\dagger is the spin transition operator from $1/2$ to $3/2$ and $\boldsymbol{\sigma}$ is the ordinary Pauli spin matrix.

The N^* self-energy due to the coupling to the πN channel is written as

$$\Sigma_{\pi N}(\sqrt{s}) = \frac{f_{\pi NN^*}^2}{2(m+M)} \int_0^\infty dp \frac{p^2 e^{-2(p/p_{\pi NN^*})^2}}{\sqrt{s} - \omega_\pi(p) - E_N(p) + i\epsilon} \left(\frac{p}{p_{\pi NN^*}}\right)^4. \quad (2.5)$$

This expression is derived by using the vertex function of Eq.(2.3).

The N^* self-energy due to the coupling to the s-wave or d-wave $\pi\Delta$ channel is expressed in a similar fashion,

$$\Sigma_{\pi\Delta}^{s(d)}(\sqrt{s}) = \int \frac{d^3p}{(2\pi)^3} \frac{1}{2\omega_\pi(p)} \frac{F_{\pi\Delta N^*}^{s(d)} F_{\pi\Delta N^*}^{s(d)\dagger}}{\sqrt{s} - \omega_\pi(p) - E_\Delta(p) - \Sigma_\Delta^{(\pi N)}(p, \sqrt{s})}, \quad (2.6)$$

where $E_\Delta = \sqrt{(M_\Delta^0)^2 + |\mathbf{p}|^2}$ and M_Δ^0 is the bare mass of Δ . $\Sigma_\Delta^{(\pi N)}$ is the Δ self-energy due to the coupling to the πN channel, which expression is given in Ref. [21]. We employ the same $\pi N\Delta$ vertex function and bare mass of Δ used by Betz and Lee [22]. The vertex functions for the $N^* \rightarrow \pi\Delta$ are defined as

$$F_{\pi\Delta N^*}^{s\dagger}(p) = -i(2\pi)^{3/2} \sqrt{\frac{2\omega_\pi(p)}{2(m+M)}} f_{\pi\Delta N^*}^s e^{-(p/p_{\pi\Delta N^*}^s)^2} Y_{00}(\hat{\mathbf{p}}), \quad (2.7)$$

$$F_{\pi\Delta N^*}^{d\dagger}(p) = -i(2\pi)^{3/2} \sqrt{\frac{2\omega_\pi(p)}{2(m+M)}} f_{\pi\Delta N^*}^d \left(\frac{p}{p_{\pi\Delta N^*}^d}\right)^2 e^{-(p/p_{\pi\Delta N^*}^d)^2} \left(S_{3/2}^{(2)\dagger} \cdot Y_2(\hat{\mathbf{p}})\right), \quad (2.8)$$

where s and d denote s-wave and d-wave $\pi\Delta$ states, and $f_{\pi N^* \Delta}^s$ and $f_{\pi\Delta N^*}^d$ are the s-wave and d-wave $N^* \rightarrow \pi\Delta$ coupling constants, respectively. $p_{\pi\Delta N^*}^{s,d}$ are the $\pi\Delta N^*$ range parameters. The spin transition operator from $3/2$ to $3/2$, $S_{3/2}^{(2)\dagger}$, in Eq.(2.8) is defined by

$$\left\langle \frac{3}{2}m' \left| S_{3/2\mu}^{(2)\dagger} \right| \frac{3}{2}m \right\rangle = \left(\frac{3}{2}m2\mu \left| \frac{3}{2}m' \right. \right), \quad (2.9)$$

where $(j_1m_1j_2m_2|JM)$ is the corresponding Clebsch-Gordan coefficient.

The N^* self-energy due to the coupling to the ρN channel is written as

$$\Sigma_{\rho N}(\sqrt{s}) = \int \frac{d^3p}{(2\pi)^3} \frac{M}{2\omega_\rho(p)E_N(p)} \frac{F_{\rho NN^*}F_{\rho NN^*}^\dagger}{\sqrt{s} - \omega_\rho(p) - E_N(p) - \Sigma_{\rho\pi\pi}(p, \sqrt{s})}, \quad (2.10)$$

where $\omega_\rho(p) = \sqrt{(m_\rho^0)^2 + |\mathbf{p}|^2}$ and m_ρ^0 is the bare mass of the ρ -meson. The vertex function for the $N^* \rightarrow \rho N$ is

$$F_{\rho NN^*}^\dagger = (2\pi)^{3/2} \sqrt{\frac{2\omega_\rho(p)E_N(p)}{M}} f_{\rho NN^*} e^{-(p/p_{\rho NN^*})^2} (\mathbf{S}^\dagger \cdot \boldsymbol{\varepsilon}_\rho) Y_{00}(\hat{\mathbf{p}}), \quad (2.11)$$

where $\boldsymbol{\varepsilon}_\rho$ is the ρ -meson polarization vector and $p_{\rho NN^*}$ is the ρNN^* range parameter, $f_{\rho NN^*}$ is the ρNN^* coupling constant. $\Sigma_{\rho\pi\pi}$ in Eq.(2.10) is the ρ -meson self-energy which is due to the coupling to the $\pi\pi$ state. The $\rho\pi\pi$ vertex function is assumed to take form:

$$F_{\rho\pi\pi} = 2h_\rho(\kappa)(\boldsymbol{\varepsilon}_\rho \cdot \boldsymbol{\kappa}), \quad (2.12)$$

$$h_\rho(\kappa) = \frac{f_{\rho\pi\pi}}{1 + (\kappa/q_{\rho\pi\pi})^2}, \quad (2.13)$$

where $q_{\rho\pi\pi}$ is the $\rho\pi\pi$ range parameter and $f_{\rho\pi\pi}$ is the $\rho\pi\pi$ coupling constant. Using this vertex function, $\Sigma_{\rho\pi\pi}$ is written as

$$\Sigma_{\rho\pi\pi}(p, \sqrt{s}) = \frac{1}{12\pi^2\omega_\rho(p)} \int_0^\infty d\kappa \frac{\kappa^4}{\omega_\pi^2(\kappa)} \frac{(h_\rho(\kappa))^2}{\sqrt{s} - E_N(p) - \sqrt{4\omega_\pi^2(\kappa) + p^2} + i\epsilon} f_\kappa, \quad (2.14)$$

where $f_\kappa = 2\omega_\pi(\kappa)/\sqrt{4\omega_\pi^2(\kappa) + p^2}$. The above expression for the ρ -meson self-energy is obtained by extending the self-energy in the rest frame of ρ to that in the moving frame. It should be noted that the imaginary part of Eq.(2.14) has a right form of the half width for the ρ -meson with the momentum p ,

$$\frac{\Gamma_{\rho\pi\pi}(p, \sqrt{s})}{2} = \frac{1}{24\pi\omega_\rho(p)} \frac{\kappa_e^3}{\omega_\pi(\kappa_e)} (h_\rho(\kappa_e))^2, \quad (2.15)$$

where κ_e satisfies $\sqrt{s} - E_N(p) - \sqrt{4\omega_\pi^2(\kappa_e) + p^2} = 0$. When m_ρ^0 is replaced by the on-shell ρ -meson mass and $q_{\rho\pi\pi}$ is taken to be infinite, Eq.(2.15) is reduced to the width of Ref. [15].

In order to calculate the self-energy of the ρ -meson, one needs to know three independent parameters, i.e., $f_{\rho\pi\pi}$, $q_{\rho\pi\pi}$ and m_ρ^0 . These parameters can not be determined uniquely by using the mass and width of the ρ -meson. Therefore, we treat the parameter $q_{\rho\pi\pi}$ as a free parameter and vary it to reproduce the $\gamma p \rightarrow \pi^+ \pi^0 n$ data. If $q_{\rho\pi\pi}$ is fixed, m_ρ^0 and $f_{\rho\pi\pi}$ are determined by the following condition,

$$m_\rho^{\text{exp}} - \left(m_\rho^0 + \Sigma_{\rho\pi\pi}(0, m_\rho^{\text{exp}} + M) \right) \approx i \frac{154}{2} \text{ [MeV]}, \quad (2.16)$$

where $m_\rho^{\text{exp}} \approx 770$ MeV.

The self-energies and bare masses of Δ and ρ in the N^* -propagator are obtained through the data such as the πN P_{33} scattering, the resonance energies and their widths in a phenomenological way as mentioned above. So there are nine parameters which have to be determined: the coupling constants ($f_{\pi NN^*}$, $f_{\pi\Delta N^*}^s$, $f_{\pi\Delta N^*}^d$, $f_{\rho NN^*}$), the range parameters ($p_{\pi NN^*}$, $p_{\pi\Delta N^*}^s$, $p_{\pi\Delta N^*}^d$, $p_{\rho NN^*}$) and the bare mass ($M_{N^*}^0$). We determine the parameters by fitting them to branching ratios, the N^* resonance energy, its width and the energy dependence of the πN D_{13} scattering amplitude. In our model, we use 1520 MeV as the resonance energy and 120 MeV as the width. We take a fraction of 58% for the decay into πN , 10% into s-wave $\pi\Delta$, 10% into d-wave $\pi\Delta$ and 22% decay into the ρN channel, respectively.

The parameters obtained are given in Table I. The parameter-set (I), (II) and (III) have been obtained by using Eq.(2.12) with $q_{\rho\pi\pi} = \infty$, 100 MeV/c and 200 MeV/c, respectively. In the parameter-set (I), the self-energy and the bare mass of ρ in Eq.(2.10) have been assumed to be the width and the on-shell mass, respectively, which corresponds to the treatment of Ref. [15]. One finds that the πN D_{13} partial-wave amplitude can be equivalently reproduced by any parameter-set in Table I. It should be noted that the sign of coupling constants is not determined from the data, since coupling constants appear as their squared form in the self-energy. Which parameter-set and which sign are appropriate will be discussed in Sec.V.

III. γNN^* COUPLING

In this section, we show how to determine the γNN^* coupling constants. Obviously, the γNN^* vertex has two independent helicity couplings. For the proton target, the helicity 1/2 amplitude is small enough compared with the helicity 3/2 amplitude. Hence, helicity 1/2 amplitude could be neglected [10–12]. For the neutron target, on the other hand, one can not use this approximation, since the helicity 1/2 amplitude is non-negligible.

The resonant amplitude in the isobar model has the form

$$T_{N^*}^{\gamma N} = F_{\pi NN^*} \frac{1}{\sqrt{s} - M_{N^*} - \Sigma_{\text{total}}} F_{\gamma NN^*}^\dagger, \quad (3.1)$$

where $F_{\gamma NN^*}$ is the vertex function for the $\gamma N \rightarrow N^*$ transition. For the helicity 1/2 transition, $F_{\gamma NN^*}^\dagger$ is written as

$$F_{\gamma NN^*}^{1/2\dagger} = -ig_{1/2} (\mathbf{S}^\dagger \cdot \hat{\mathbf{k}}) (\boldsymbol{\sigma} \cdot \hat{\mathbf{k}} \times \boldsymbol{\varepsilon}), \quad (3.2)$$

where $g_{1/2}$ and $\boldsymbol{\varepsilon}$ are the helicity 1/2 coupling constant and photon polarization vector, respectively, and $\hat{\mathbf{k}}$ denotes the unit vector of initial photon momentum. In our approximation, this helicity coupling constant for the proton is set to zero. The helicity 3/2 transition $F_{\gamma NN^*}^\dagger$ operator is written as

$$F_{\gamma NN^*}^{3/2\dagger} = g_{3/2} \left\{ (\mathbf{S}^\dagger \cdot \boldsymbol{\varepsilon}) + \frac{i}{2} (\mathbf{S}^\dagger \cdot \hat{\mathbf{k}}) (\boldsymbol{\sigma} \cdot \hat{\mathbf{k}} \times \boldsymbol{\varepsilon}) \right\}, \quad (3.3)$$

where $g_{3/2}$ is the helicity 3/2 coupling constant.

The relevant multipole amplitudes can not be described by only the resonant form of Eq.(3.1) since there is a non-negligible background process. Actually, the full D_{13} amplitude should be expressed as the sum of two terms, i.e., the background and the N^* resonant terms (Fig.1) [23,24],

$$T(D_{13}) = T_B + \tilde{T}_{N^*}, \quad (3.4)$$

$$\tilde{T}_{N^*} = F_{\pi NN^*} \frac{1}{\sqrt{s} - M_{N^*} - \Sigma_{\text{total}}} \tilde{F}_{\gamma NN^*}^{1/2,(3/2)\dagger}, \quad (3.5)$$

where T_B is the non-resonant multipole amplitude which is obtained from the partial-wave decomposition of the Born term in the $\gamma N \rightarrow \pi N$ reaction. The γNN^* vertex function is rewritten as

$$\tilde{F}_{\gamma NN^*}^{1/2(3/2)\dagger} = \tilde{g}_{1/2(3/2)}(\sqrt{s}) \frac{F_{\gamma NN^*}^{1/2(3/2)\dagger}}{g_{1/2(3/2)}}, \quad (3.6)$$

where $\tilde{g}_{1/2(3/2)}$ represents the effective helicity $1/2$ ($3/2$) coupling constant, which includes the contribution of the N^* production through the πN , $\pi\Delta$ and ρN intermediate states (Fig.2 (c) to (e)) in addition to the direct production (Fig. 2 (b)). This coupling constant is complex and energy dependent.

The effective γNN^* coupling constant $\tilde{g}_{1/2(3/2)}$ is phenomenologically determined by through a fit to the experimental multipole amplitudes of Refs. [10–12], instead of calculating the diagrams of Fig.2 (c),(d) and (e) in a microscopic way. Here we use the Born term with the same coupling constants and cutoff employed by Nozawa *et al.* [24]. If the multipole amplitude of Ref. [12] is used, for example, the helicity $3/2$ coupling constant for the proton target becomes $\tilde{g}_{3/2} = 0.1621 + i0.0522$ at 750 MeV photon energy.

IV. MODEL OF THE $\gamma N \rightarrow \pi\pi N$ REACTION

The total cross section for the $\gamma N \rightarrow \pi^1\pi^2 N$ reaction is given by

$$\sigma = \frac{1}{2k} \frac{M}{E_i} \frac{1}{v_s} \int \frac{d^3 p_f}{(2\pi)^3} \frac{d^3 q_1}{(2\pi)^3} \frac{d^3 q_2}{(2\pi)^3} \frac{M}{E_f} \frac{1}{2\omega_\pi(q_1)} \frac{1}{2\omega_\pi(q_2)} \times (2\pi)^4 \delta^{(4)}(p_i + k - p_f - q_1 - q_2) \sum_{\nu\nu'} \frac{1}{2} |\langle 1/2, \nu | T | 1/2, \nu' \rangle|^2, \quad (4.1)$$

where $p_i = (E_i, \mathbf{p}_i)$, $p_f = (E_f, \mathbf{p}_f)$ and $q_a = (\omega_\pi, \mathbf{q}_a)$ ($a = 1, 2$) are the initial nucleon, the final nucleon and the final pion ($\pi^{1,2}$) 4-momenta in the center-of-mass system, respectively, and v_s is the relative velocity of the initial nucleon and the photon. The absolute square of the invariant matrix element T for the $\gamma N \rightarrow \pi\pi N$ reaction is summed over the final nucleon spin states (ν') and averaged over the initial nucleon spin states (ν).

We describe how the matrix element T in Eq.(4.1) is derived within our approach. We assume that the $\gamma N \rightarrow \pi\pi N$ reaction is dominated by the processes of the $\gamma N \rightarrow \pi\Delta \rightarrow \pi\pi N$

and the $\gamma N \rightarrow N^* \rightarrow \pi\pi N$. In this assumption, there are four important processes shown in Figs.3(a),(b),(c) and (d). We neglect other possible diagrams involving Δ , which are obtained from the requirement of the gauge invariance, since these contributions has been shown to be small [15].

The diagram (a) in Fig.3 contains the $\gamma N \pi \Delta$ contact term, i.e., the Δ Kroll-Ruderman term. This $\gamma N \pi \Delta$ contact term operator $F_{\Delta\text{KR}}^\dagger$ is obtained from the strong $\pi N \Delta$ vertex function by requiring the gauge invariance. Instead of using the effective Lagrangian [15], we start from the vertex function with a form factor. The $N \rightarrow \pi \Delta$ transition operator $F_{\pi N \Delta}^\dagger$ is assumed to be the same form with the $\Delta \rightarrow \pi N$ vertex function which is phenomenologically given in Ref. [22]. Since the range parameter Q_Δ (see Appendix) may not be necessarily the same, we treat it as a free parameter and vary it to fit the $\gamma p \rightarrow \pi^+ \pi^- p$ cross section (see Table I). Its matrix element in coordinate space in non-relativistic limit is given by (suppressing the isospin factor)

$$\begin{aligned} \langle \pi \Delta | F_{\pi \Delta N}^\dagger | N \rangle = & \int d^3 r_N d^3 \rho \left\{ \Psi_\Delta^\dagger(\mathbf{r}_N - \frac{m_\pi}{M_{\pi\Delta}} \boldsymbol{\rho}) \Phi_\pi^\dagger(\mathbf{r}_N + \frac{m_\pi}{M_{\pi\Delta}} \boldsymbol{\rho}) \right\} \\ & (+i)(\mathbf{S}^\dagger \cdot \vec{\nabla}_\rho) H(\rho) \Psi_N(\mathbf{r}_N), \end{aligned} \quad (4.2)$$

where \mathbf{r}_N and $\boldsymbol{\rho}$ are the $\pi \Delta$ center-of-mass and relative coordinates, respectively, and $M_{\pi\Delta} = M_\Delta + m$. The $\pi N \Delta$ form factor H is given in Appendix. The Δ and pion wave functions in Eq.(4.2) may be expanded around \mathbf{r}_N in power series of the relative coordinate $\boldsymbol{\rho}$. If all gradients with respect to \mathbf{r}_N operating on the Δ and pion wave functions are replaced by $\nabla_N - ie_\Delta \mathbf{A}(\mathbf{r}_N)$ or $\nabla_N - ie_\pi \mathbf{A}(\mathbf{r}_N)$, where e_Δ and e_π are the Δ and pion electric charges, the resulting vertex function is invariant under the gauge transformation [25]. The electromagnetic interaction for the $\gamma N \rightarrow \pi \Delta$ process is then derived by the expansion to order \mathbf{A} . Simplifying this interaction further according to the prescription described in Ref. [25], we obtain

$$F_{\Delta\text{KR}}^\dagger = -i \left\{ G_1(|\mathbf{q}_a|) (\mathbf{S}^\dagger \cdot \boldsymbol{\varepsilon}) + G_2(|\mathbf{q}_a|) (\mathbf{S}^\dagger \cdot \boldsymbol{\kappa}) (\boldsymbol{\kappa} \cdot \boldsymbol{\varepsilon}) \right\}. \quad (4.3)$$

This expression, i.e., the minimal interaction current, is employed in our model. Here, masses

of the pion and the Δ in Eq.(4.2) are replaced by their energies as the relativistic generalization and the $\gamma N\pi\Delta$ form factors G_1 , G_2 are defined in Appendix. The first term in the left-hand side of Eq.(4.3) corresponds to the ordinary contact term (the Δ Kroll-Ruderman term). The second term, on the other hand, appears due to the presence of the $\pi N\Delta$ form factor. It should be noted that the above minimal interaction current has a contribution to the $\gamma p\pi^0\Delta^+$ vertex because of the charged Δ , although there is no contribution within the framework of the effective Lagrangian. As shown later, this interaction has a small but non-negligible effect on the $\gamma p \rightarrow \pi^0\pi^0p$ cross section.

In our model, the $\gamma N\pi\Delta$ pion-pole term $F_{\Delta\text{PP}}^\dagger$ included in Fig.3(b) will be derived from the time-ordered perturbation theory. The vertex functions for the $\Delta \rightarrow \pi N$ and $N \rightarrow \pi\Delta$ transitions are of the same form as that in Eq.(4.2). But the range parameter Q_Δ of the latter is taken to be the same as that of Eq.(4.3). The operator $F_{\Delta\text{PP}}^\dagger$ is then written as

$$F_{\Delta\text{PP}}^\dagger = \frac{ig_p}{\omega_\pi(|\mathbf{q}_a - \mathbf{k}|)} \left\{ \frac{H(\kappa_1)}{D_\Delta(q_a, E_N(k) - \omega_\pi(|\mathbf{q}_a - \mathbf{k}|))} (\mathbf{S}^\dagger \cdot \boldsymbol{\kappa}_1) - \frac{H(\kappa_2)}{k - \omega_\pi(q_a) - \omega_\pi(|\mathbf{q}_a - \mathbf{k}|)} (\mathbf{S}^\dagger \cdot \boldsymbol{\kappa}_2) \right\} (\mathbf{q}_a \cdot \boldsymbol{\varepsilon}), \quad (4.4)$$

where

$$\boldsymbol{\kappa}_1 = \mathbf{q}_a - \frac{\omega_\pi(|\mathbf{q}_a - \mathbf{k}|)\mathbf{k}}{E_\Delta(q_a) + \omega_\pi(|\mathbf{q}_a - \mathbf{k}|)}, \quad (4.5)$$

$$\boldsymbol{\kappa}_2 = \mathbf{k} - \frac{\omega_\pi(|\mathbf{q}_a - \mathbf{k}|)\mathbf{q}_a}{E_N(q_a) + \omega_\pi(|\mathbf{q}_a - \mathbf{k}|)}, \quad (4.6)$$

$$D_\Delta(p, E) = E - E_\Delta(p) - \Sigma_\Delta^{(\pi N)}(p, E). \quad (4.7)$$

Here, $\boldsymbol{\kappa}_1$ and $\boldsymbol{\kappa}_2$ are the $\pi\Delta$ and πN relative momenta and $\Sigma_\Delta^{(\pi N)}(p, E)$ is the self-energy of Δ with the momentum p . The charge-dependent factor g_p is given in Appendix.

Using Eqs.(4.3) and (4.4), we can write the invariant matrix element for the diagrams of Fig.3(a) and (b) in the following.

$$T_{\Delta\text{KR},(\text{PP})} = \frac{F_{\pi N\Delta} F_{\Delta\text{KR},(\text{PP})}^\dagger}{\sqrt{s} - \omega_\pi(q) - E_\Delta(q) - \Sigma_\Delta^{(\pi N)}(q, \sqrt{s})}, \quad (4.8)$$

where $T_{\Delta\text{KR}}$ and $T_{\Delta\text{PP}}$ represent the Δ Kroll-Ruderman term and Δ pion-pole term, respectively. Multiplying Eq.(4.8) by appropriate isospin factors, we get the T -matrix elements

for various reactions.

For the $\gamma N \rightarrow N^* \rightarrow \pi\pi N$ process, there are two possible processes accompanied with either the $N^* \rightarrow \pi\Delta$ or $N^* \rightarrow \rho N$ decay as shown in Figs.3(c) and (d). The N^* resonance can decay into both s-wave and d-wave $\pi\Delta$ states. In order to construct the T -matrix involving the N^* , we use the strong and electromagnetic vertex functions obtained in Secs.II and III. Using Eqs.(2.7), (2.8), (2.11), (2.12) and (3.6), the T -matrix elements of Fig. 3(c) and (d) are written as

$$T_{N^*(\pi\Delta)}^{\text{s(d)-wave}} = \frac{F_{\pi N \Delta} F_{\pi \Delta N^*}^{s(d)\dagger} \tilde{F}_{\gamma N N^*}^\dagger}{(\sqrt{s} - \omega_\pi(q) - E_\Delta(q) - \Sigma_\Delta^{(\pi N)}(q, \sqrt{s})) (\sqrt{s} - M_{N^*} - \Sigma_{\text{total}})}, \quad (4.9)$$

$$T_{N^*(\rho N)} = \frac{F_{\rho\pi\pi} F_{\rho N N^*} \tilde{F}_{\gamma N N^*}^\dagger}{2\omega_\rho(q) (\sqrt{s} - \omega_\rho(q) - E_N(q) - \Sigma_{\rho\pi\pi}(q, \sqrt{s})) (\sqrt{s} - M_{N^*} - \Sigma_{\text{total}})}, \quad (4.10)$$

respectively.

Therefore, the invariant matrix element T in Eq.(4.1) is expressed as follows:

$$T = T_{\Delta\text{KR}} + T_{\Delta\text{PP}} + T_{N^*(\pi\Delta)}^{\text{s-wave}} + T_{N^*(\pi\Delta)}^{\text{d-wave}} + T_{N^*(\rho N)}. \quad (4.11)$$

V. NUMERICAL RESULTS AND DISCUSSION

In this section, we present our calculations of the total cross sections for the $\gamma N \rightarrow \pi\pi N$ reaction, which are shown in Figs.4 to 6. We calculated them with the parameters obtained in previous sections, but the sign of some strong coupling constants and the range parameter $Q_\Delta(N \rightarrow \pi\Delta)$ will be determined so as to fit them to the $\gamma p \rightarrow \pi^+ \pi^- p$ data. Then, we will discuss which parameters of the $\rho\pi\pi$ form factor are favored by the $\gamma p \rightarrow \pi^+ \pi^0 n$ data. In our numerical calculations, the Monte Carlo integration package BASES25 [26] is used.

At first, we show the results of $\gamma p \rightarrow \pi^+ \pi^- p$ and $\gamma n \rightarrow \pi^+ \pi^- n$ reaction cross sections (solid lines) in Figs.4-(i) and (ii) which are calculated with the parameter-set (I) in Table I. As can be seen from Fig.4-(i), the Δ Kroll-Ruderman term $T_{\Delta\text{KR}}$ and Δ pion-pole term $T_{\Delta\text{PP}}$ terms (dashed line) dominate on the $\gamma p \rightarrow \pi^+ \pi^- p$ reaction. We observe that the N^* contribution (dash-dotted line) alone is small but the interference between the N^* term

$T_{N^*(\pi\Delta)}^{\text{s-wave}}$ and $T_{\Delta\text{KR}}$ is important. This strong interference occurs due to the fact that $T_{N^*(\pi\Delta)}^{\text{s-wave}}$ has the same structure as $T_{\Delta\text{KR}}$. Because of this, the N^* excitation is regarded as an important ingredient in the $\gamma p \rightarrow \pi\pi N$ reaction.

As mentioned in Sec.II, there is an ambiguity about the sign of strong coupling constants, $f_{\pi\Delta N^*}^{s,d}$ and $f_{\rho NN^*}$. We adopt a positive sign for $f_{\pi\Delta N^*}^s$ which gives rise to a constructive interference between $T_{N^*(\pi\Delta)}^{\text{s-wave}}$ and $T_{\Delta\text{KR}}$. The peak position of the $\gamma p \rightarrow \pi^+\pi^-p$ cross section can be reproduced with this choice as shown in Fig.4-(i). We find that the curve with $f_{\pi\Delta N^*}^s > 0$, $f_{\pi\Delta N^*}^d < 0$, and $f_{\rho NN^*} < 0$ agrees well with the $\gamma p \rightarrow \pi^+\pi^-p$ data [13,14,17,18]. The range parameter $Q_\Delta(N \rightarrow \pi\Delta)$ is taken to be 420 MeV/c. Hereafter, we will use the same sign for the coupling constants. Furthermore, the $\gamma n \rightarrow \pi^+\pi^-n$ reaction cross section (Fig.4-(ii)) is calculated by using the same parameter-set (I) except for the γNN^* coupling. Our calculation with this parameter-set is also in good agreement with the $\gamma n \rightarrow \pi^+\pi^-n$ data [17,18]. This is different from the result by Tejedor *et al.* [15]. Their model could not reproduce the $\gamma n \rightarrow \pi^+\pi^-n$ data in spite of good agreement with the $\gamma p \rightarrow \pi^+\pi^-p$ data. This difference may be attributed mainly to the theoretical treatment of the Δ Kroll-Ruderman term. In any case, new experiments for the neutron target would be welcome in order to check the validity of our model.

Secondly, we show the results of the $\gamma p \rightarrow \pi^+\pi^0n$ and $\gamma n \rightarrow \pi^-\pi^0p$ reactions in Figs.5-(i) and (ii) (thin-solid lines), which are calculated with the parameter-set (I). In both reactions, we find a large discrepancy with the data [14,17,18]. Our model underestimates cross sections about a factor of two compared with the data. In these reactions, as shown in Fig.5-(i) and (ii), $T_{\Delta\text{KR}}$ and $T_{\Delta\text{PP}}$ contribution (short-dashed line) is very small. We also find that the contribution of the N^* terms (dash-dotted line) is almost the same as that in the $\gamma p \rightarrow \pi^+\pi^-p$ reaction but there is no characteristic energy-dependence due to the interference which is clearly observed in the $\gamma p \rightarrow \pi^+\pi^-p$ cross section. This can be understood by the isospin factor. The isospin ratio of the $T_{\Delta\text{KR(PP)}}$ term of the $\gamma p \rightarrow \pi^+\pi^0n$ reaction to the $\gamma p \rightarrow \pi^+\pi^-p$ reaction is

$$\frac{T_{\Delta\text{KR(PP)}}(\pi^+\Delta^0 \rightarrow \pi^+\pi^0n)}{T_{\Delta\text{KR(PP)}}(\pi^-\Delta^{++} \rightarrow \pi^-\pi^+p)} = -\frac{\sqrt{2}}{3}, \quad (5.1)$$

where only the intermediate and final states are written in the invariant matrix element T but the initial state γN is omitted. For instance, $T(\pi^-\Delta^{++} \rightarrow \pi^+\pi^-p)$ means $T(\gamma p \rightarrow \pi^-\Delta^{++} \rightarrow \pi^+\pi^-p)$. Eq.(5.1) indicates that the cross section for the $\gamma p \rightarrow \pi^+\pi^0n$ reaction is $2/9$ times smaller than $\gamma p \rightarrow \pi^+\pi^-p$ reaction. This feature is not changed even if other small terms are included. The isospin ratio of the $T_{N^*(\pi\Delta)}^{\text{s(d)-wave}}$ term of the $\gamma p \rightarrow \pi^+\pi^0n$ to $\gamma p \rightarrow \pi^+\pi^-p$ reaction is

$$\frac{T_{N^*(\pi\Delta)}^{\text{s(d)-wave}}(\pi^+\Delta^0 \rightarrow \pi^+\pi^0n)}{T_{N^*(\pi\Delta)}^{\text{s(d)-wave}}(\pi^-\Delta^{++} \rightarrow \pi^-\pi^+p)} = \frac{1}{\sqrt{2}}. \quad (5.2)$$

Eqs.(5.1) and (5.2) show that a relative sign between $T_{\text{KR(PP)}}$ and $T_{N^*(\pi\Delta)}^{\text{s-wave}}$ in the $\gamma p \rightarrow \pi^+\pi^0n$ reaction is different from that in the $\gamma p \rightarrow \pi^+\pi^-p$ reaction, and Eq.(5.2) indicates that $T_{N^*(\pi\Delta)}^{\text{s-wave}}$ in the $\gamma p \rightarrow \pi^+\pi^0n$ reaction is smaller than that in $\gamma p \rightarrow \pi^+\pi^-p$ reaction. Therefore, the interference between T_{KR} and $T_{N^*(\pi\Delta)}^{\text{s-wave}}$ in the $\gamma p \rightarrow \pi^+\pi^0n$ reaction is different from that in the $\gamma p \rightarrow \pi^+\pi^-p$ reaction. In addition, there is another important feature regarding the ρ -production amplitude (diagram (d) in Fig.3). The isospin ratio of the $T_{N^*(\rho N)}$ term is

$$\frac{T_{N^*(\rho N)}(\rho^+n \rightarrow \pi^+\pi^0n)}{T_{N^*(\rho N)}(\rho^0p \rightarrow \pi^-\pi^+p)} = \sqrt{2}. \quad (5.3)$$

The Eq.(5.3) shows that the $T_{N^*(\rho N)}$ term in the $\gamma p \rightarrow \pi^+\pi^0n$ reaction is larger than that in the $\gamma p \rightarrow \pi^+\pi^-p$ reaction. Hence, the ρ -meson production term is important in the $\gamma p \rightarrow \pi^+\pi^0n$ reaction. The large shift of the peak compared with the calculation of the $\gamma p \rightarrow \pi^+\pi^-p$ cross section may be due to the large $T_{N^*(\rho N)}$ term. The same arguments remain true for the $\gamma n \rightarrow \pi^+\pi^-n$ and $\gamma n \rightarrow \pi^-\pi^0p$ reactions.

As can be seen from Figs.4-(i),(ii), Figs.5-(i) and (ii)(thin-solid lines), one finds that our model is successful in the $\gamma N \rightarrow \pi^+\pi^-N$ reaction but fails to reproduce the experimental results of the $\gamma p \rightarrow \pi^+\pi^0n$ and $\gamma n \rightarrow \pi^-\pi^0p$ reactions. This difficulty concerning the π^0 production has been already pointed out in other studies [15,16]. In order to improve our model and resolve this problem, we examine the two possible processes shown in Figs.3 (e)

and (f), which may contribute more effectively to the $\gamma p \rightarrow \pi^+ \pi^0 n$ than the $\gamma p \rightarrow \pi^+ \pi^- p$ reaction. The diagram (e) in Fig.3 is the final state rescattering process. But we found from our rough estimate that the cross section for this rescattering diagram (e) is very small.

Next, let us discuss the effect of the diagram (f) in Fig.3 in detail. This diagram contributes only to the $\gamma p \rightarrow \pi^+ \pi^0 n$ and $\gamma n \rightarrow \pi^- \pi^0 p$ reactions, since it contains $\gamma N \rho N$ contact interaction (ρ -Kroll-Ruderman term). The invariant matrix element for this diagram is written as

$$T_{\rho\text{KR}} = \frac{F_{\rho\pi\pi} F_{\gamma N \rho N}^\dagger}{2\omega_\rho(q)(\sqrt{s} - \omega_\rho(q) - E_N(q) - \Sigma_{\rho\pi\pi}(q, \sqrt{s}))}. \quad (5.4)$$

Here $F_{\gamma N \rho N}^\dagger$ represents the $\gamma N \rho N$ contact term

$$F_{\gamma N \rho N}^\dagger = ie f_c \frac{G^T}{2M} \boldsymbol{\epsilon}_\rho \cdot (\boldsymbol{\sigma} \times \boldsymbol{\epsilon}), \quad (5.5)$$

where $G^T = -17.6$ is the tensor coupling to the ρNN channel and the factor f_c is taken to be $\sqrt{m_\rho^0 m'_\rho / (m_\rho^{\text{exp}})^2}$. $m'_\rho = m_\rho^0 + \Sigma_{\rho\pi\pi}(0, M)$ is the mass of ρ carrying zero momentum and zero energy. The factor f_c arises from the fact that the intermediate ρ -meson mass in our model is different from the on-shell mass. The effect of this factor is however small so that it does not affect our final results significantly. Thus, our new invariant matrix element T matrix becomes

$$T = T_{\Delta\text{KR}} + T_{\Delta\text{PP}} + T_{N^*(\pi\Delta)}^{\text{s-wave}} + T_{N^*(\pi\Delta)}^{\text{d-wave}} + T_{N^*(\rho N)} + T_{\rho\text{KR}}. \quad (5.6)$$

We neglect the other possible diagram obtained by requiring the gauge invariance, i.e., the ρ -meson pole diagram, since its effect was found to be negligible.

In order to see the effect of the diagram (f) in Fig.3, we calculated the $\gamma p \rightarrow \pi^+ \pi^0 n$ cross section by using the invariant matrix element T of Eq.(5.6), which is shown as dotted line in Fig.5-(i). In this calculation, we used the parameter-set (I). As far as $T_{\rho\text{KR}}$ term is concerned, in this case, the theoretical treatment in our model is essentially the same with the model by Murphy *et al.* [16]. From the comparison between the calculation with $T_{\rho\text{KR}}$ (dotted line) and without $T_{\rho\text{KR}}$ (thin-solid line), the contribution of the diagram (f) in Fig.3 is found to be very small, which is consistent with the result of Ref. [16].

To improve our model, we will treat the ρ -meson propagator in a dynamical way since the ρ -meson involved in the double pion photoproduction is not on-shell below the energy range 800 MeV. We allow the range parameter of the $\rho\pi\pi$ form factor to be finite as described in Sec. II. We calculate the cross section with the parameter-set (II) in Table I where the range parameter of the $\rho\pi\pi$ form factor $q_{\rho\pi\pi}$ is 100 MeV/c and $Q_\Delta(N \rightarrow \pi\Delta)$ is 400 MeV/c. For the $\gamma p \rightarrow \pi^+\pi^-p$ cross section, the result with the parameter-set (II) is almost the same as that with the parameter-set (I). As can be seen from Fig.5-(i), however, the significant enhancement occurs in the cross section of the $\gamma p \rightarrow \pi^+\pi^0n$ reaction (bold-solid line). Our improved model fairly well reproduces the data of the $\gamma p \rightarrow \pi^+\pi^0n$ reaction, except for the energy region above 750 MeV. This result is quite different from those by Tejedor *et al.* [15] and Murphy *et al.* [16]. Furthermore, we have calculated the $\gamma n \rightarrow \pi^-\pi^0p$ reaction cross section by using the same parameter-set. The calculation is shown in Fig.5-(ii)(bold-solid line). We find that our model with this parameter-set is also able to reproduce the experimental data for the neutron target [17,18].

In order to find the reason why such significant enhancement has occurred, we plot a 2π -spectral function, i.e., $\text{Im}\Sigma_{\rho\pi\pi}/|\sqrt{s} - m_\rho - \Sigma_{\rho\pi\pi}|^2$ which is proportional to the integrated cross section for the diagram (f). The curves with the range parameter $q_{\rho\pi\pi} = 100$ (solid line), 200 (dashed line), 300 (dash-dotted line) MeV/c, respectively, are plotted in Fig.7. The peak is clearly seen at the ρ -meson resonance energy. Furthermore, below the 400 MeV, there is a small bump in the curve with $q_{\rho\pi\pi} = 100$ MeV/c. This non-negligible effect may cause a significant enhancement to the $\gamma p \rightarrow \pi^+\pi^0n$ reaction cross section. One can see the similar enhancement in the 2π -spectral function associated with the $N\bar{N} \rightarrow 2\pi$ reaction in Ref. [27]. This low-energy behavior comes from the background contribution in the isospin $I = 1$ channel. Our model for the 2π scattering includes only the $\rho\pi\pi$ coupling, but not the background interaction. However, the small range parameter in our model might simulate the background interaction effectively.

We show the results of double neutral pion photoproduction processes in Figs.6-(i) and (ii). As can be seen from Fig.6-(i), the peak position of the calculated cross section of the

$\gamma p \rightarrow \pi^0 \pi^0 p$ is in good agreement with the data [14]. On the other hand, the magnitude of the cross section is underestimated about a factor of two. Murphy *et al.* suggested [16] that the $\gamma p \rightarrow \pi^0 \pi^0 p$ reaction cross section was enhanced by the presence of the $P_{11}(1440)$ resonance which decays into the σ -meson. However, it seems that other important mechanisms are still missing. We leave this problem as a next step since we are interested in the total photoabsorption at present. We also show the $\gamma n \rightarrow \pi^0 \pi^0 n$ reaction cross section in Fig.6-(ii). Unfortunately, there are no experimental data to compare with our calculation.

Finally, we show the total photoabsorption cross sections (solid lines) for γp and γn reactions in Figs.8-(i) and (ii), respectively. We assume that the total photoabsorption off a nucleon is dominated by the $\gamma N \rightarrow \pi N$ and $\gamma N \rightarrow \pi\pi N$ reactions in the energy region where we discuss. The $\gamma N \rightarrow \pi N$ cross sections (dashed lines) are calculated by using the amplitude given in Ref. [12] except for the D_{13} amplitude. The D_{13} amplitude is treated in the same way described in Secs.II and IV. On the other hand, the $\gamma N \rightarrow \pi\pi N$ reaction cross sections (dash-dotted lines) are calculated by using our model with the parameter-set (II). We found our model reproduces the experimental data both γp [4,28] and γn [29] reactions over the wide range of the energy. We should mention that the double neutral pion photoproduction scarcely contribute to the total photoabsorption cross section.

VI. CONCLUSION

We have constructed a simple model for the $\gamma N \rightarrow \pi\pi N$ reaction. It is assumed in this model that the processes of $\gamma N \rightarrow \pi\Delta(1232)$, $\gamma N \rightarrow N^*(1520)$ and $\gamma N \rightarrow \rho N$ are dominant in the double pion production. We treat the resonances such as Δ , N^* and ρ -meson in a dynamical way.

The $\gamma N\pi\Delta$ contact operator is derived from the strong $\pi N\Delta$ vertex function by requiring the gauge invariance, instead of the effective Lagrangian. The range parameter of the $N \rightarrow \pi\Delta$ form factor in this operator is determined so as to reproduce the $\gamma p \rightarrow \pi^+\pi^- p$ data. For the Δ resonance, the dynamical model by Betz and Lee [22] was used. We have carefully

discussed the dynamical model for the N^* resonance because this resonance plays very important roles in the energy range where we concern. The strong vertex functions of πNN^* , $\pi\Delta N^*$ and ρNN^* are obtained from the πN scattering amplitudes, decay widths and the resonance energy of N^* . The sign of each strong coupling constant is not determined from only the above data. However, as the sign affects the energy dependence of the double pion photoproduction cross section, it could be fixed to reproduce the $\gamma p \rightarrow \pi^+ \pi^- p$ data. The electromagnetic couplings of γNN^* are determined through a fit to the $\gamma N \rightarrow \pi N$ D_{13} helicity 1/2 and 3/2 partial-wave amplitude.

Our model with the above parameters can simultaneously reproduce total cross sections of both the $\gamma p \rightarrow \pi^+ \pi^- p$ and $\gamma n \rightarrow \pi^+ \pi^- n$ reactions. We found that the Δ Kroll-Ruderman term and the Δ pion-pole term had a dominant contribution to these reactions and the interference between the Δ Kroll-Ruderman term and the N^* term was very important to explain the energy-dependence of the cross sections.

For the $\gamma p \rightarrow \pi^+ \pi^0 n$ and $\gamma n \rightarrow \pi^- \pi^0 p$ reactions, on the other hand, the contributions of the Δ Kroll-Ruderman term and the Δ pion-pole term are smaller compared with the $\gamma N \rightarrow \pi^+ \pi^- N$ reaction. In order to reproduce the $\gamma p \rightarrow \pi^+ \pi^0 n$ data, we found that one should treat the ρ -meson in a dynamical model where the $\rho\pi\pi$ vertex has a finite-ranged form factor. In fact, it has turned out in our calculation with the appropriate range parameter that the $\gamma N \rho N$ contact term contributes to these π^0 productions significantly. As a result, our improved model could simultaneously reproduce both the $\gamma p \rightarrow \pi^+ \pi^0 n$ and $\gamma n \rightarrow \pi^- \pi^0 p$ cross sections, except for the energy region above 750 MeV. The disagreement at higher energy may be due to the fact that other higher resonances are not taken into account in our model.

The total cross section of the $\gamma p \rightarrow \pi^0 \pi^0 p$ reaction is underestimated about a factor of two. Still some important mechanisms are missing in our model. We leave this problem as a next step.

Finally, we have calculated the total cross sections of the photoabsorption off a nucleon. We found that our model is able to reproduce the experimental results of the proton target

as well as the neutron target. The defect of our model regarding the double neutral pion production gives little influence on the total photoabsorption cross section, since the magnitude of its cross section is very small. As far as the total cross section is concerned, we consider that our model has a predictable power for nuclear processes. Based on our model, we are investigating the mechanism which has caused the resonance damping in the nuclear photoabsorption [30].

ACKNOWLEDGMENTS

We are grateful to Dr. N. Aizawa for instructing us BASES25. We also thank Prof. Y. Sumi for indication of nuclear photoabsorption data.

APPENDIX A: THE $\pi N\Delta$ AND $\gamma N\pi\Delta$ FORM FACTORS

The $\pi N\Delta$ form factor H is defined as

$$H(q) = \sqrt{6\pi^2} \sqrt{\frac{2\omega_\pi(q)E_N(q)}{M}} g_{\pi N\Delta}(q), \quad (\text{A1})$$

where $g_{\pi N\Delta}$ is given by [22]

$$g_{\pi N\Delta} = \frac{F_\Delta}{\sqrt{2(m+M)}} \frac{q}{m} \left(\frac{Q_\Delta^2}{Q_\Delta^2 + q^2} \right)^2, \quad (\text{A2})$$

where F_Δ is the coupling constant and Q_Δ is the range parameter. The $\gamma N\pi\Delta$ form factor G_1 and G_2 in Eq.(4.3) and the factor g_p in Eq.(4.4) are given as follows.

1) $\gamma p \rightarrow \pi^- \Delta^{++}$ reaction

$$G_1 = e \{ Z_2 H(|\mathbf{q} - Z_2 \mathbf{k}|) + 2Z_3 H(|\mathbf{q} + Z_3 \mathbf{k}|) \}, \quad (\text{A3})$$

$$G_2 = e(-\tilde{h}_\pi + 2\tilde{h}_\Delta), \quad (\text{A4})$$

$$g_p = -2e. \quad (\text{A5})$$

2) $\gamma p \rightarrow \pi^+ \Delta^0$ reaction

$$G_1 = -\frac{e}{\sqrt{3}} Z_2 H(|\mathbf{q} - Z_2 \mathbf{k}|), \quad (\text{A6})$$

$$G_2 = -\frac{e}{\sqrt{3}} \tilde{h}_\pi, \quad (\text{A7})$$

$$g_p = \frac{2}{\sqrt{3}} e. \quad (\text{A8})$$

3) $\gamma p \rightarrow \pi^0 \Delta^+$ reaction

$$G_1 = -\frac{e}{\sqrt{3}} Z_3 H(|\mathbf{q} + Z_3 \mathbf{k}|), \quad (\text{A9})$$

$$G_2 = -\sqrt{\frac{2}{3}} e \tilde{h}_\Delta, \quad (\text{A10})$$

$$g_p = 0 \quad (\text{A11})$$

4) $\gamma n \rightarrow \pi^+ \Delta^-$ reaction

$$G_1 = e \{ -Z_2 H(|\mathbf{q} - Z_2 \mathbf{k}|) - Z_3 H(|\mathbf{q} + Z_3 \mathbf{k}|) \}, \quad (\text{A12})$$

$$G_2 = e(\tilde{h}_\pi - \tilde{h}_\Delta), \quad (\text{A13})$$

$$g_p = 2e. \quad (\text{A14})$$

5) $\gamma n \rightarrow \pi^- \Delta^+$ reaction

$$G_1 = \frac{e}{\sqrt{3}} \{ Z_2 H(|\mathbf{q} - Z_2 \mathbf{k}|) + Z_3 H(|\mathbf{q} + Z_3 \mathbf{k}|) \}, \quad (\text{A15})$$

$$G_2 = \frac{e}{\sqrt{3}} (\tilde{h}_\Delta - \tilde{h}_\pi), \quad (\text{A16})$$

$$g_p = -\frac{2}{\sqrt{3}} e. \quad (\text{A17})$$

where e is electromagnetic charge and including isospin Clebsch-Gordan coefficients of the $\gamma N \pi \Delta$ vertex, and

$$Z_2 = \frac{E_\Delta(q)}{E_\Delta(q) + \omega(q)}, \quad (\text{A18})$$

$$Z_3 = \frac{\omega(q)}{E_\Delta(q) + \omega(q)}, \quad (\text{A19})$$

$$\tilde{h}_\pi = \frac{H(|\mathbf{q} - Z_2 \mathbf{k}|) - H(q)}{\mathbf{k} \cdot (\mathbf{q} - Z_2 \mathbf{k}/2)}, \quad (\text{A20})$$

$$\tilde{h}_\Delta = \frac{H(|\mathbf{q} + Z_3 \mathbf{k}|) - H(q)}{\mathbf{k} \cdot (\mathbf{q} + Z_3 \mathbf{k}/2)}. \quad (\text{A21})$$

REFERENCES

- [1] M. Anghinolfi *et al.*, Phys. Rev. C **47** (1993) R992.
- [2] N. Bianchi *et al.*, Phys.Lett. B **229** (1993) 219.
- [3] N. Bianchi *et al.*, Phys. Lett. B **309** (1993) 5.
- [4] M. MacCormick *et al.*, Phys. Rev. C **53** (1996) 41.
- [5] N. Bianchi *et al.*, Phys. Rev. C**54** (1996) 1688.
- [6] W.M. Alberico, G. Gervino and A. Lavagno, Phys. Lett. B 321. (1994) 177
- [7] L.A. Kondratyuk, M.I. Krivoruchenko, N. Bianchi, E. De Sanctis, V. Mucchifora, Nucl. Phys. A **579** (1994) 453.
- [8] M. Effenberger, A. Hombach, S. Teis and U. Mosel, preprint nucl-th/9607005.
- [9] see, for example, C. Betourne *et al.*, Phys. Rev. **172** (1968) 11343, S.D. Ecklund and R.L. Walker, *ibid.* **159** (1967) 1195, H. De Staebler *et al.*, *ibid.* **140** (1965) B337.
- [10] R.G. Moorhouse, H. Oberlack and A.H. Rosenfeld, Phys. Rev. D **9** (1974) 1.
- [11] I. Arai and H. Fujii, Nucl. Phys. **B194** (1982) 251.
- [12] R.A. Arndt, R.L. Workman, Z. Li and L.D. Roper, Phys. Rev. C **42** (1990) 1853, and the Scattering Analysis Interactive Dial-in (SAID) program, available by TELNET call to `clsaid.phys.vt.edu`, or WWW site at <http://clsaid.phys.vt.edu>.
- [13] Aachen-Berlin-Bonn-Hamburg-Heidelberg-München collaboration, Phys. Rev. **175** (1968) 1669.
- [14] A. Braghieri *et al.*, Phys. Lett. B **365** (1995) 46 .
- [15] J.A.G. Tejedor, E. Oset, Nucl. Phys. A**571** (1994) 667, preprint hep-ph/9506209.
- [16] L.Y. Murphy and J.M. Laget, preprint DAPNIA-SPHN-95-42.

- [17] A. Piazza *et al.*, Nuovo Cimento **III** (1970) 403.
- [18] F. Carbobara *et al.*, Nuovo Cimento **36 A** (1976) 219.
- [19] Particle Data Group, Phys. Rev. D **50** (1994).
- [20] R.S. Bhalerao and L.C. Liu, Phys. Rev. Lett. **54** (1985) 865.
- [21] M. Arima, K. Masutani, R. Seki, Phys. Rev. C **51** (1995) 285.
- [22] M. Betz and T.-S.H. Lee, Phys. Rev. C **23** (1981) 375.
- [23] J.H. Koch, E.J. Moniz, and N. Ohtsuka, Ann. Phys. **154** (1984) 99.
- [24] S. Nozawa, B. Blankleider and T.-S.H. Lee, Nucl. Phys. A **513** (1990) 459.
- [25] L. Heller, S. Kumano, J.C. Martinez and E.J. Moniz, Phys. Rev. C **35** (1987) 718.
- [26] S. Kawabata, Comput. Phys. Commun. **41** (1986) 127.
- [27] E. Oset, H. Toki and W. Weise, Phys. Rep. **83** No.4 (1982) 281.
- [28] T.A. Armstrong, *et al.*, Phys. Rev. D **5** (1972) 1640.
- [29] T.A. Armstrong, *et al.*, Nucl. Phys. B **41** (1972) 445.
- [30] K. Ochi, M. Hirata and T. Takaki, in preparation.

TABLES

TABLE I. The parameters used in our model. Only the absolute value of coupling constants is given. The sign is discussed in the text.

	parameter-set (I)	parameter-set (II)	parameter-set (III)
M_{N^*} (MeV)	1597	1554	1566
$f_{\pi NN^*}$	1.09	1.13	1.13
$p_{\pi NN^*}$ (MeV/c)	450	400	400
$f_{\pi \Delta N^*}^s$	0.992	0.992	0.992
$p_{\pi \Delta N^*}^s$ (MeV/c)	200	200	200
$f_{\pi \Delta N^*}^d$	0.984	1.00	1.00
$p_{\pi \Delta N^*}^d$ (MeV/c)	200	300	300
$f_{\rho NN^*}$	1.56	0.928	0.583
$p_{\rho NN^*}$ (MeV/c)	200	200	300
$f_{\rho \pi \pi}$	6.14	82.0	25.6
$q_{\rho \pi \pi}$ (MeV/c)	∞	100	200
$Q_\Delta(N \rightarrow \pi \Delta)$ (MeV/c)	420	400	400
$Q_\Delta(\Delta \rightarrow \pi N)$ (MeV/c)	358	358	358

FIGURES

FIG. 1. The $\gamma N \rightarrow \pi N$ reaction in the D_{13} channel including background and N^* production. B.G. corresponds to the background term. (a) The full- D_{13} amplitude. (b) The Born term for the $\gamma N \rightarrow \pi N$ reaction. (c) The N^* resonant term through the effective γNN^* vertex.

FIG. 2. The effective γNN^* vertex. (a) The effective γNN^* vertex. (b) The bare γNN^* vertex. (c) The vertex correction due to background πN production. (d) The vertex correction due to background $\pi\Delta$ production. (e) The vertex correction due to background ρN production.

FIG. 3. The diagrams for the $\gamma N \rightarrow \pi\pi N$ reaction. (a) The Δ Kroll-Ruderman term. (b) The Δ pion-pole term. (c) The $N^* \rightarrow \pi\Delta$ contribution. (d) The $N^* \rightarrow \rho N$ contribution. (e) The final state rescattering contribution. (f) The ρ -meson Kroll-Ruderman term.

FIG. 4. Total cross sections for (i) the $\gamma p \rightarrow \pi^+\pi^-p$ and (ii) the $\gamma n \rightarrow \pi^+\pi^-n$ reactions. Solid line corresponds to the total cross section calculated with the parameter-set(I), dashed line to the contributions of the Δ Kroll-Ruderman and Δ pion-pole terms (diagrams (a) and (b) in Fig.3) and dash-dotted line to the contributions of the N^* terms (diagrams (c) and (d) in Fig.3). Experimental data are taken from Refs. [13,14,17,18].

FIG. 5. Total cross sections for (i) the $\gamma p \rightarrow \pi^+\pi^0n$ and (ii) the $\gamma n \rightarrow \pi^-\pi^0p$ reactions. Thin-solid line corresponds to the total cross section calculated by using Eq.(4.11) with the parameter-set (I) and dotted line to the total cross section calculated by using Eq.(5.6) with the parameter-set (I). Bold-solid line corresponds to the total cross section calculated by using Eq.(5.6) with the parameter-set (II), short-dashed line to the contributions of the Δ Kroll-Ruderman and Δ pion-pole terms (diagrams (a) and (b) in Fig.3), dash-dotted line to the contributions of the N^* terms (diagrams (c) and (d) in Fig.3) and long-dashed line to the contribution of the ρ -meson Kroll-Ruderman term (diagram (f) in Fig.3) including the finite-ranged form factor of $\rho\pi\pi$. Experimental data are taken from Refs. [14,17,18].

FIG. 6. Total cross sections for (i) the $\gamma p \rightarrow \pi^0 \pi^0 p$ and (ii) the $\gamma n \rightarrow \pi^0 \pi^0 n$ reactions. Solid line corresponds to the total cross section calculated by using Eq.(5.6) with the parameter-set (II), dashed line to the contributions of the Δ Kroll-Ruderman term (diagram (a) in Fig.3) and dash-dotted line to the contribution of the N^* term (diagram (c) in Fig.3). Experimental data is taken from Ref. [14].

FIG. 7. The 2π -spectral function as a function of the center-of-mass energy. Solid line corresponds to $q_{\rho\pi\pi} = 100$ MeV/c, dashed line to $q_{\rho\pi\pi} = 200$ MeV/c and dash-dotted line to $q_{\rho\pi\pi} = 300$ MeV/c.

FIG. 8. The total photoabsorption cross section of (i) the proton target and (ii) the neutron target. Solid line corresponds to the summed cross section of $\gamma N \rightarrow \pi N$ and $\gamma N \rightarrow \pi\pi N$ which are calculated in our model. Dashed line corresponds to the contribution of $\gamma N \rightarrow \pi N$, dash-dotted line to the contribution of $\gamma N \rightarrow \pi\pi N$. Experimental data are taken from Ref. [4,28,29].

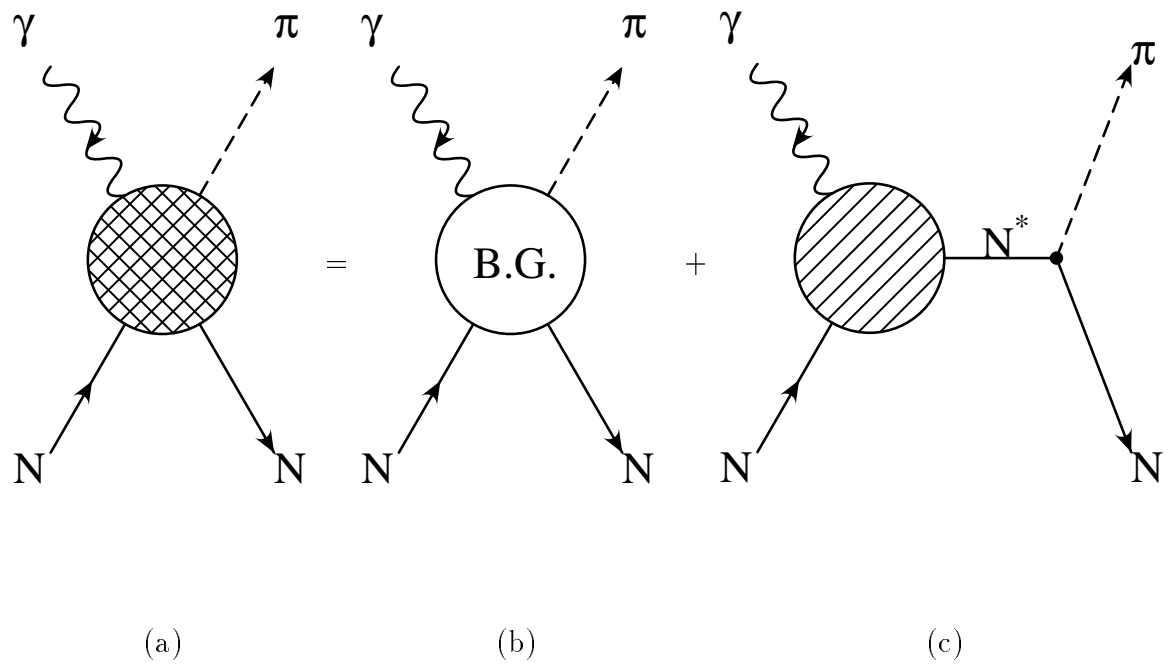


Figure 1

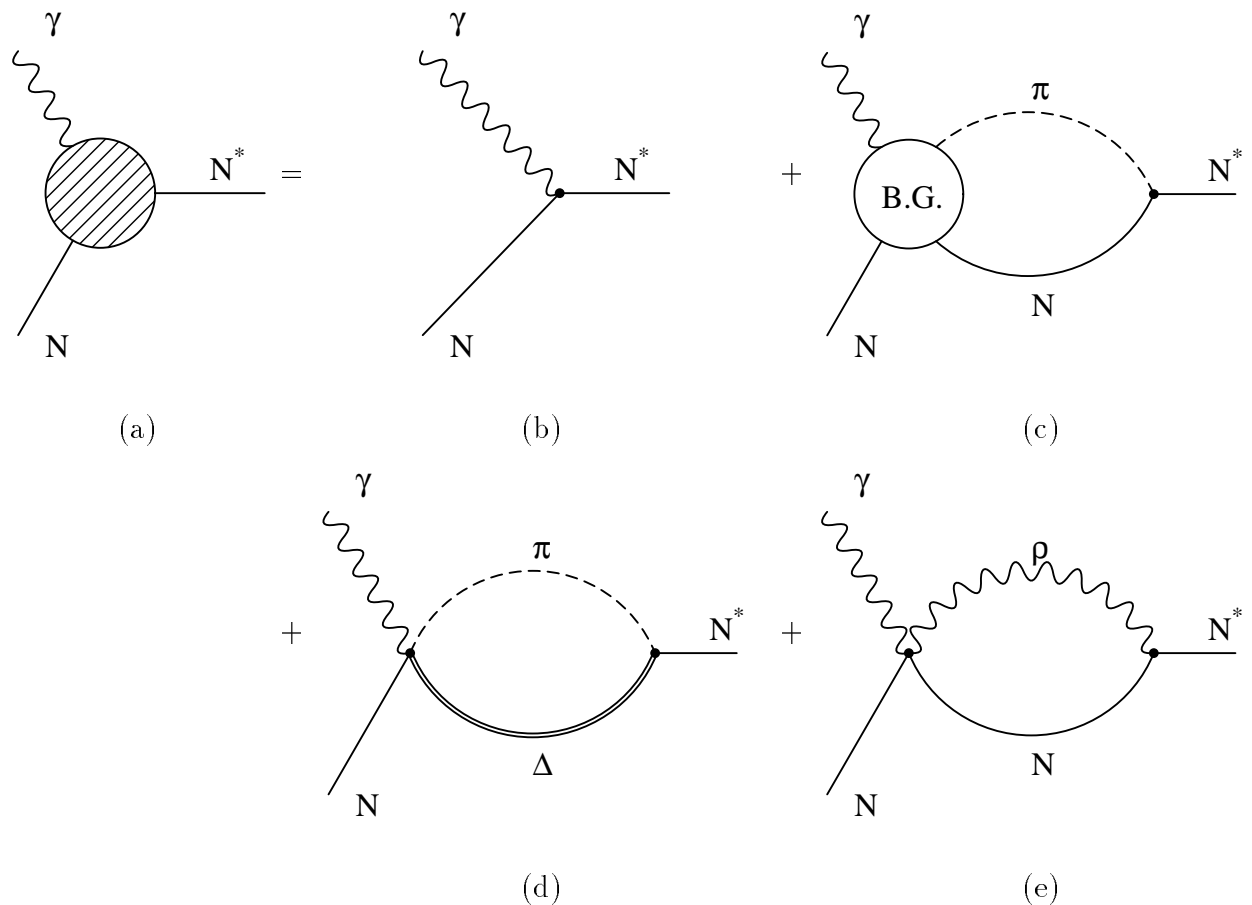
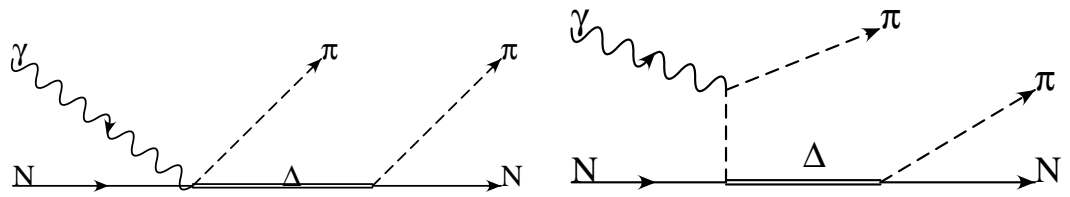
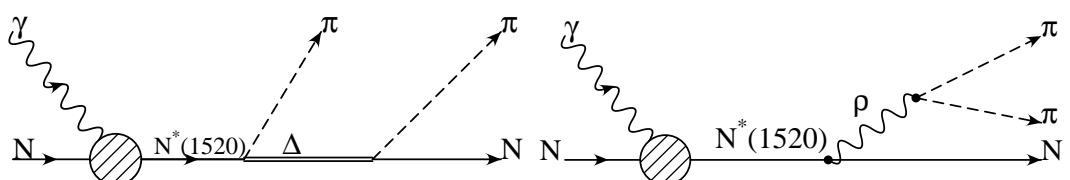


Figure 2



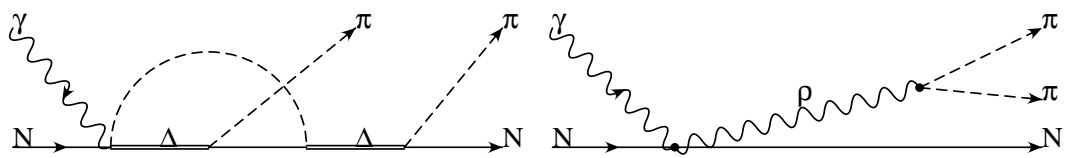
(a)

(b)



(c)

(d)



(e)

(f)

Figure 3

Figure 4-(i)

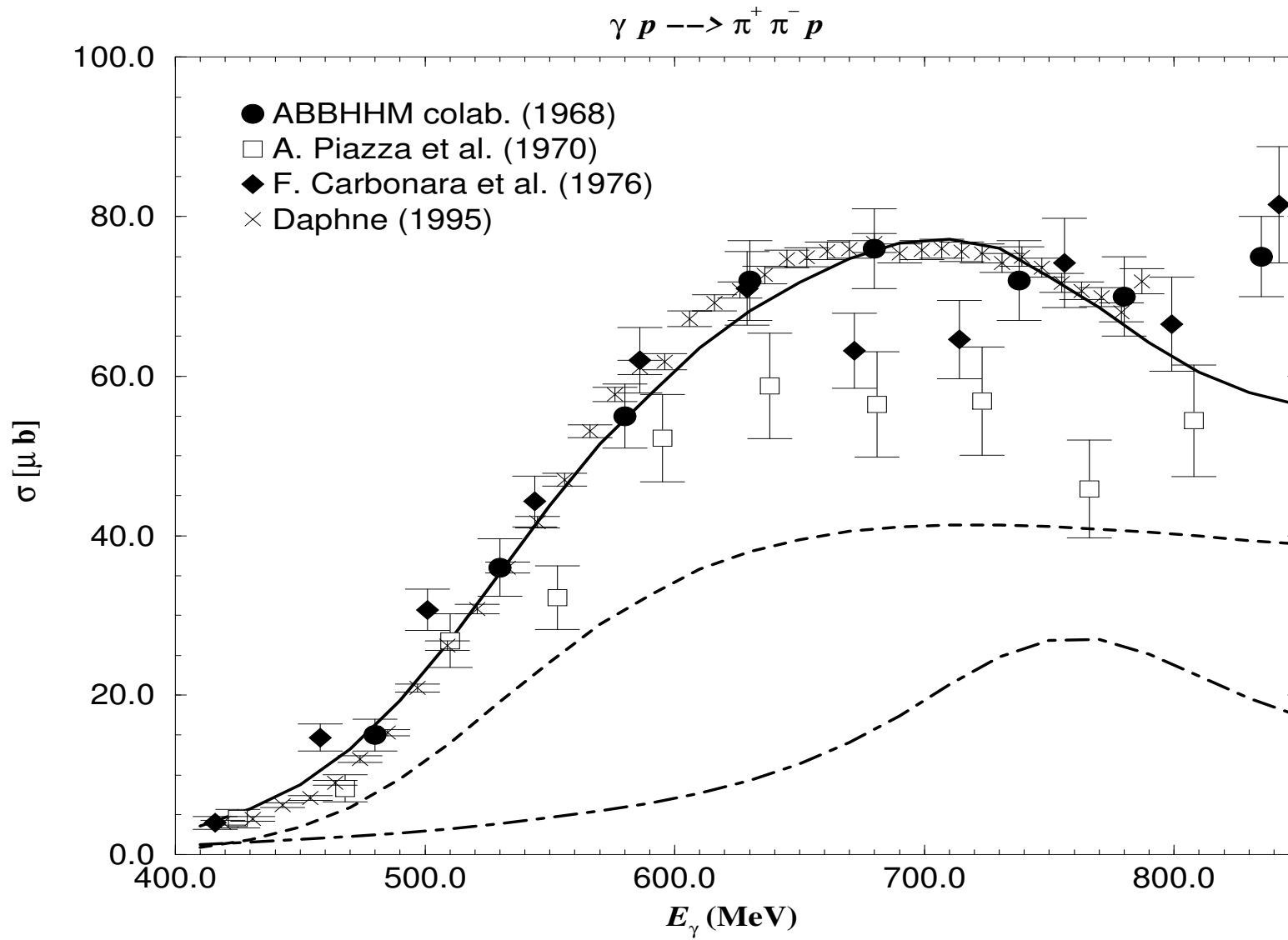


Figure 4-(ii)

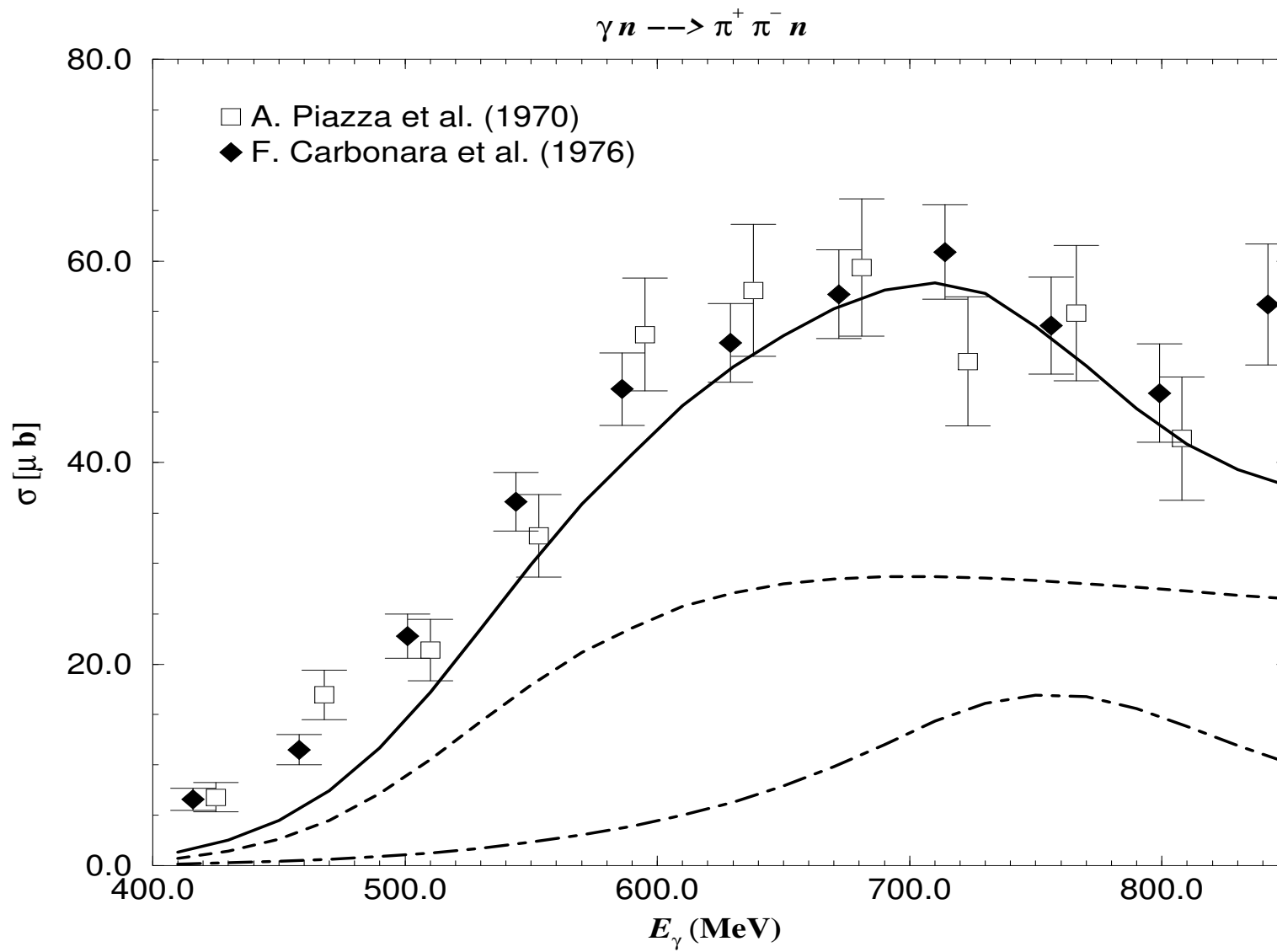


Figure 5-(i)

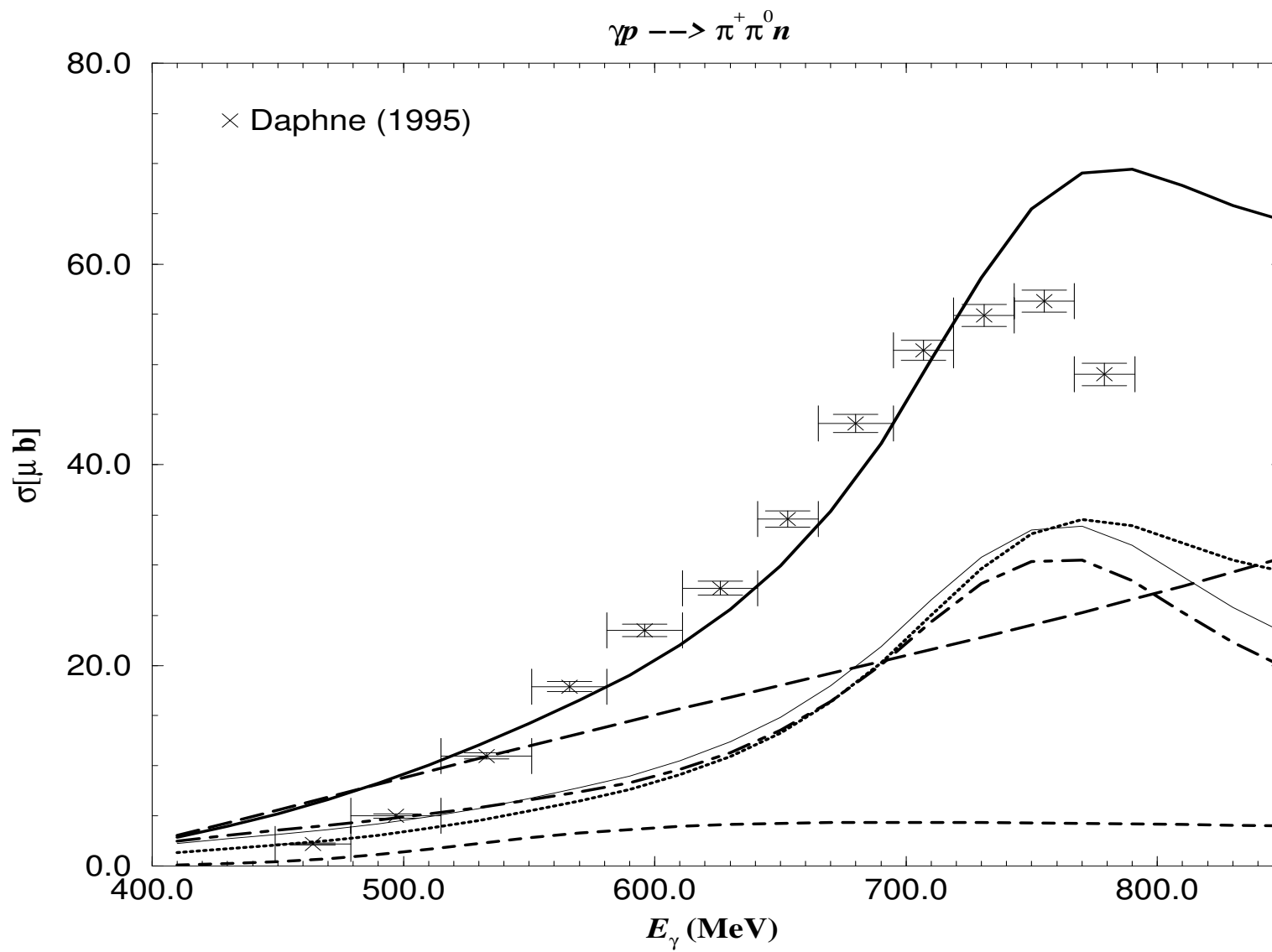


Figure 5(ii)

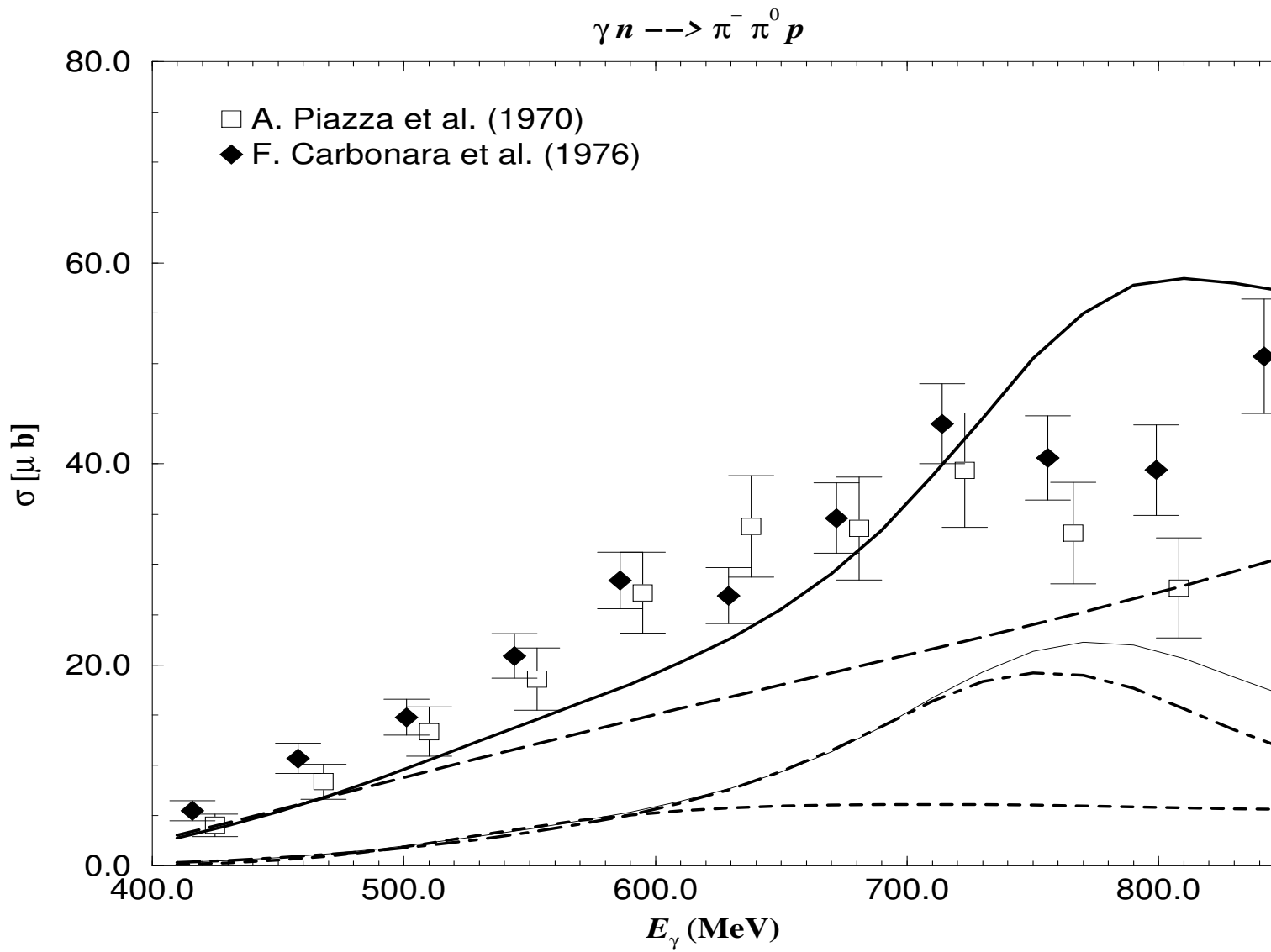


Figure 6-(i)

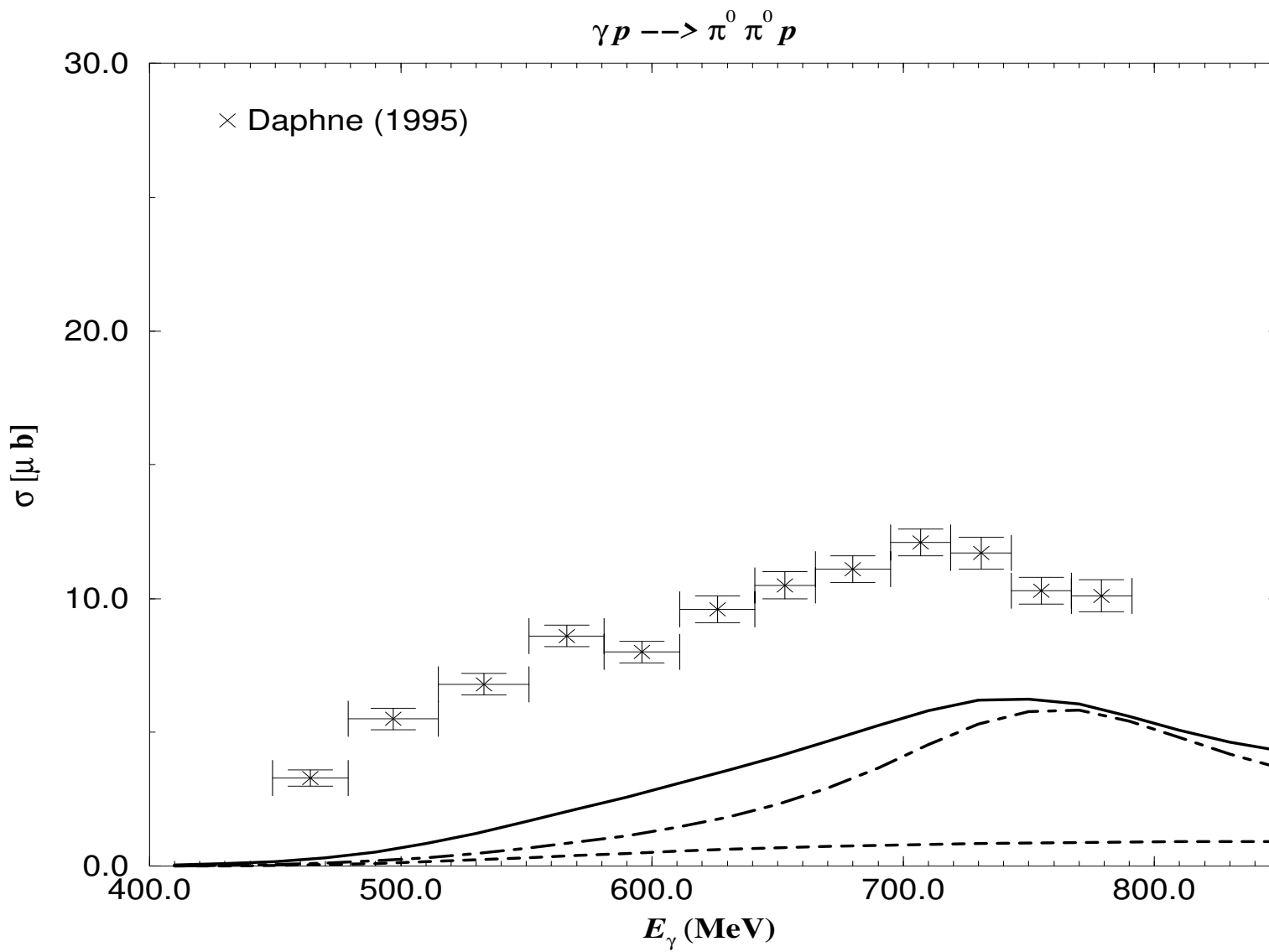


Figure 6(ii)

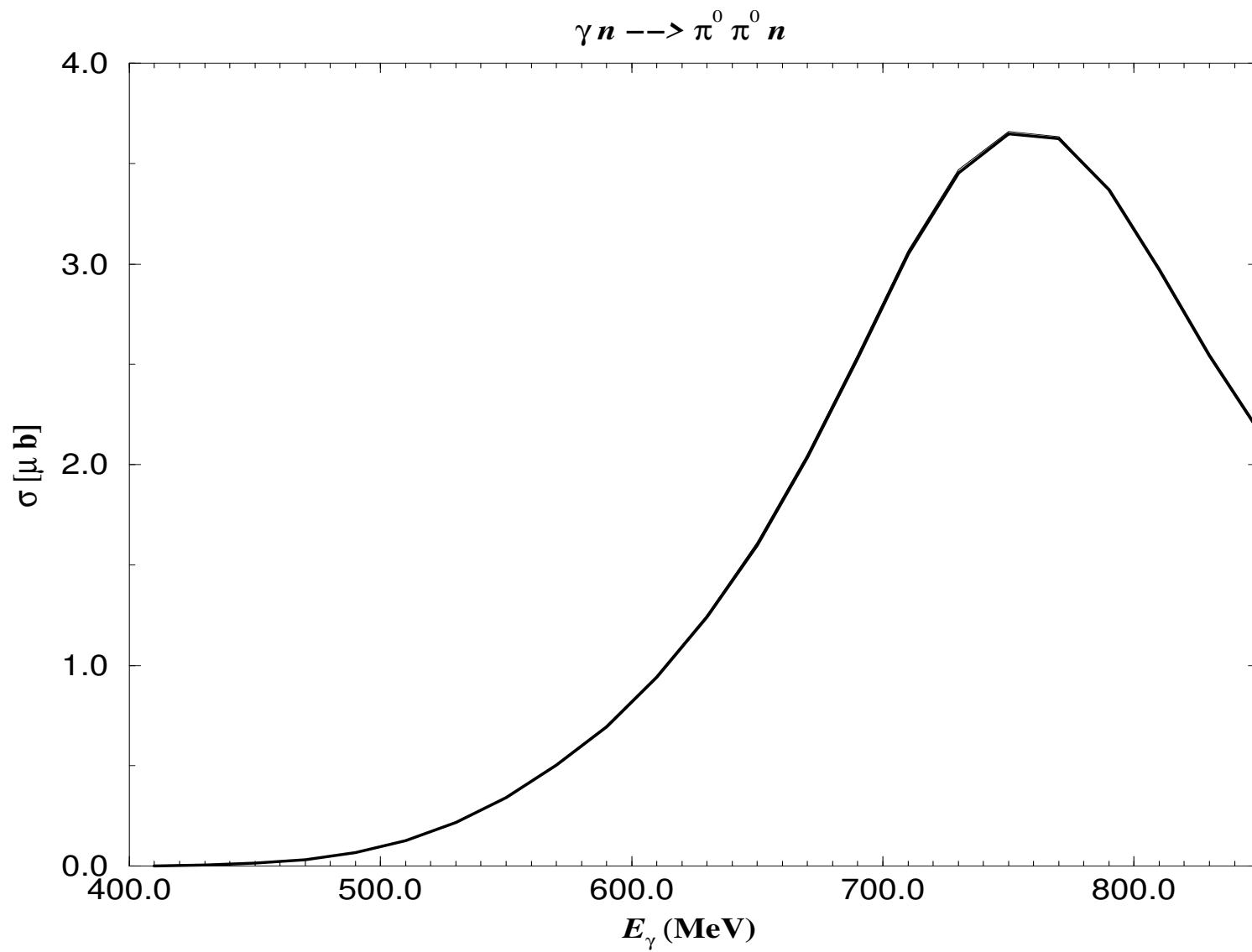


Figure 7

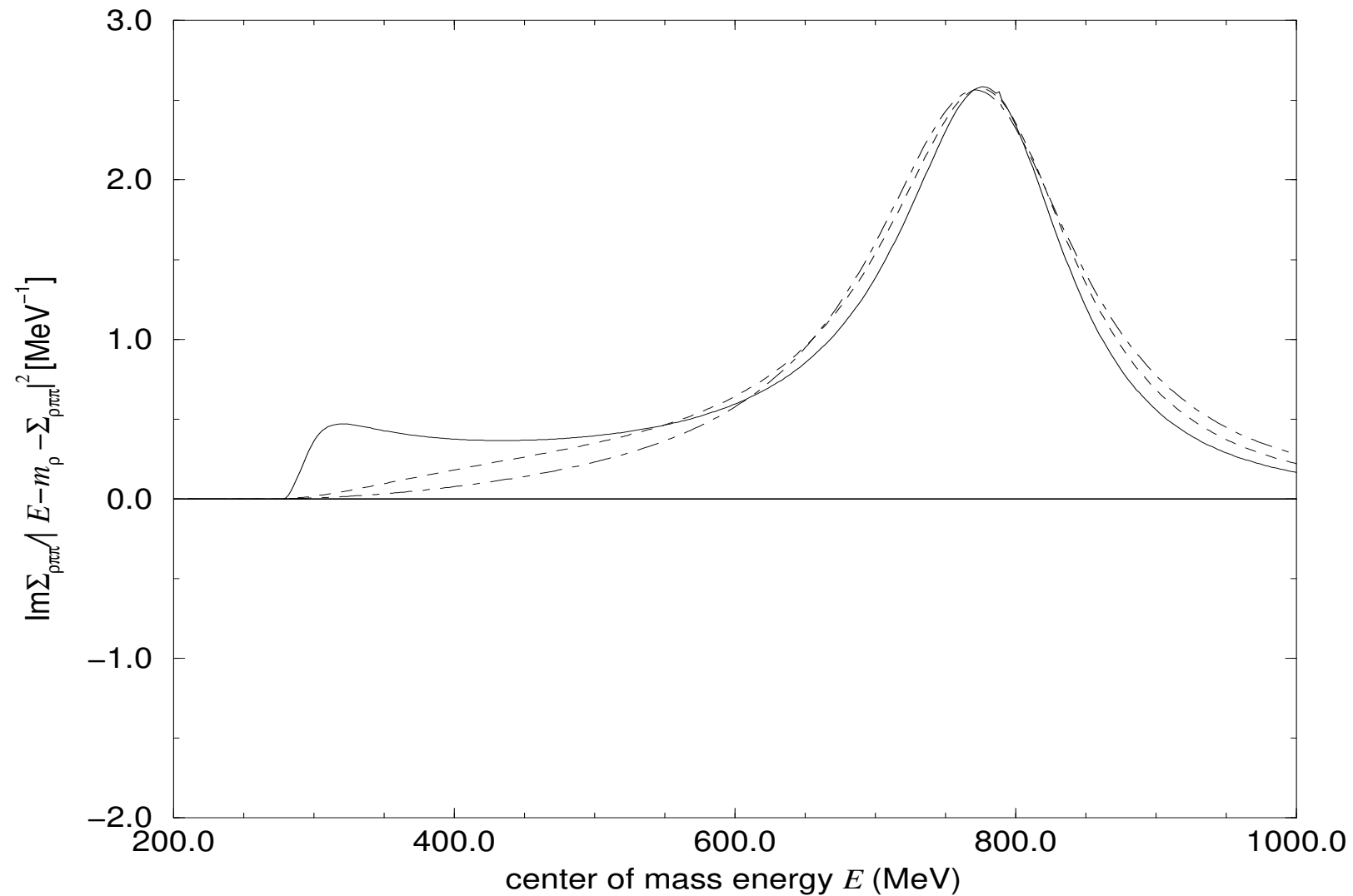


Figure 8-(i)

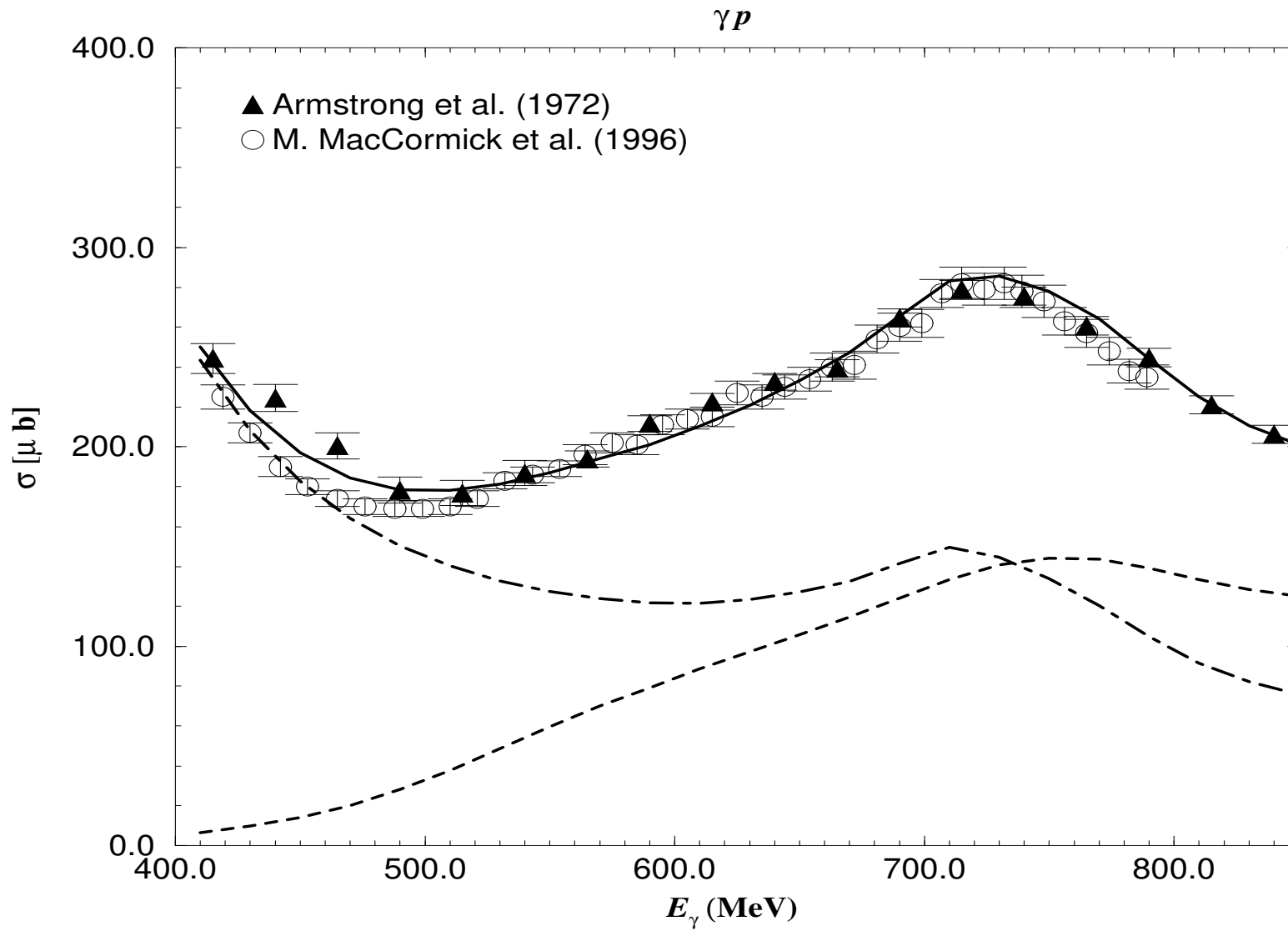


Figure 8(ii)

